Optical solitons, self-focusing, and wave collapse in a space-fractional Schrödinger equation with a Kerr-type nonlinearity

Manna Chen, Shihao Zeng, Daquan Lu, Wei Hu,[*] and Qi Guo

Guangdong Provincial Key Laboratory of Nanophotonic Functional Materials and Devices,
South China Normal University, Guangzhou 510006, China

We investigate the nonlinear dynamics of (1+1)-dimensional optical beam in the system described by the space-fractional Schrödinger equation with the Kerr nonlinearity. Using the variational method, the analytical soliton solutions are obtained for different values of the fractional Lévy index α. All solitons are demonstrated to be stable for $1 < \alpha \leqslant 2$. However, when $\alpha = 1$, the beam undergoes a catastrophic collapse (blow-up) like its counterpart in the (1+2)-dimensional system at $\alpha = 2$. The collapse distance is analytically obtained and a physical explanation for the collapse is given.

I. INTRODUCTION

The self-focusing of an optical beam [1–3], typically caused by the nonlinear optical Kerr effect, is a universal nonlinear phenomenon which can be found in almost all optical fields. It has attracted considerable interest from the pioneer age of nonlinear optics to today's latest applications, such as fiber lasers and all-optical switches. For the (1+2)-dimensional [(1+2)-D] Kerr nonlinear system, an optical beam can evolve into spikes of infinite amplitude in a finite propagation distance. This phenomenon is called wave collapse (blow-up). In the 1960s, Kelley [4] first predicted self-focusing and collapse based upon the self-trapping phenomenon, which was found by Askar'yan [5] and Chiao *et al.* [6]. Later it was experimentally observed by Lallemand *et al.* [7,8] and analytically explained by Vlasov *et al.* [9], who developed the method of moments to determine the collapse distance. Wave collapse is a fundamental physical phenomenon and has been also observed in plasma waves [10], Bose-Einstein condensates or matter waves [11], capillary-gravity waves on deep water [12], and even in astrophysics [13]. By now wave collapse has been well established in the context of the nonlinear Schrödinger equation (NLSE), which is a well-known model for all systems mentioned above. Typically it must be in two or more spatial dimensions and above a certain critical power to generate a collapse. However, in the (1+1)-dimensional [(1+1)-D] case it was recently numerically reported by Klein *et al.* that wave collapse (blow-up) can also occur in the context of a NLSE involving a fractional Laplacian of order 1/2 [14]. Here the main purpose of our study is to obtain the analytical expressions of the collapse distance and the critical power.

The fractional Schrödinger equation (FSE) in quantum mechanics was discovered by Laskin in 1999 [15–17]. This general model further stimulated interest in exploring its mathematical properties [18,19]. Recently, Longhi proposed that the FSE can describe the temporal dynamics of the transverse light field in a cavity [20]. It is commonly known that the spatial dynamics of light field can be analogous to the temporal one in mathematical analysis. The FSE, involving the first-order derivative in the evolutional coordinate z instead of the time t, has now been applied to explore the beam propagation properties. Examples include the diffraction-free beams [21], beams in an external harmonic potential [22,23] and in a parity-time symmetric potential [24], and various families of solitons [25–28]. In addition, Zhang *et al.* suggested that the real physical system described by the FSE can be potentially realized by the honeycomb lattice [29].

In this study, the features of a soliton in the FSE are investigated analytically and numerically. The stability analysis is also given and confirmed by numerical simulations. Interestingly, it is shown that the wave collapse would occur when the Lévy index $\alpha = 1$ [14]. The expressions for the collapse distance and the critical power are obtained by the variational method. Finally, the occurrence of a collapse is explained physically.

II. FRACTIONAL SCHRÖDINGER EQUATION AND ITS SOLITON SOLUTIONS

We consider the following (1+1)-D FSE:

$$i\frac{\partial}{\partial z}\Psi - \frac{1}{2}\left(-\frac{\partial^2}{\partial x^2}\right)^{\alpha/2}\Psi + |\Psi|^2\Psi = 0, \qquad (1)$$

where the transverse coordinate x is scaled by the characteristic width, and $(-\partial^2/\partial x^2)^{\alpha/2}$ represents the fractional Laplacian with α ($1 < \alpha \leqslant 2$) being the Lévy index. Equation (1) can describe two different physical situations. In the first, based on the light temporal dynamical theory developed in Ref. [20], z represents time which is normalized to the round-trip transit time in a cavity, and here $|\Psi|^2\Psi$ stands for a thin nonlinear slab instead of a phase mask. In the second, similar to the model in Refs. [14,22,23,27], z represents the propagation distance scaled by the Rayleigh range, and Eq. (1) describes the evolution of a paraxial beam $\Psi(x, z)$ in a Kerr medium. Here we mainly discuss the latter situation. For $\alpha = 2$, Eq. (1) is

---

*Corresponding author: huwei@scnu.edu.cn
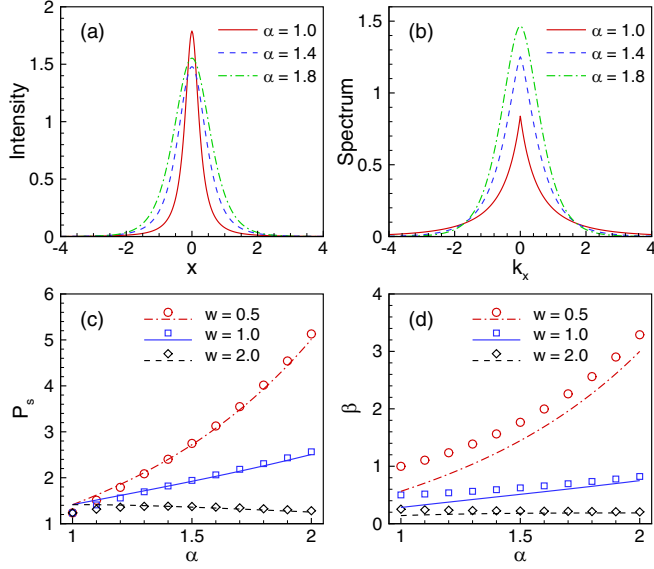
FIG. 1. Intensity profiles (a) and their Fourier spectra (b) of solitons for $w = 1$ when $\alpha = 1.0$, 1.4, and 1.8. Soliton power P_s (c) and propagation constant β (d) versus Lévy index α for $w = 0.5$, 1.0, and 2.0 (curves: the analytical results obtained by the variational method; symbols: the numerical results).

reduced to the well-known NLSE. It is easy to demonstrate that the beam power $P = \int |\Psi(x, z)|^2 dx$ is conserved for Eq. (1).

Note that Eq. (1) admits a scale transformation, i.e., if $\Psi(x, z)$ is a solution of Eq. (1), then $\Psi' = \eta^{\alpha/2}\Psi(\eta x, \eta^\alpha z)$, with a free parameter η, is also a solution. We look for stationary solutions of Eq. (1) in the form, $\Psi(x, z) = \psi(x)\exp(i\beta_0 z)$, where β_0 is the propagation constant of the soliton. The profile $\psi(x)$ is real and satisfies

$$-\frac{1}{2}\left(-\frac{\partial^2}{\partial x^2}\right)^{\alpha/2}\psi + \psi^3 = \beta_0\psi. \quad (2)$$

Using the scale invariance, its soliton solutions form a family described by

$$\Psi(x, z) = \eta^{\alpha/2}\psi(\eta x)\exp(i\eta^\alpha\beta_0 z). \quad (3)$$

The parameter $1/\eta$ is a characteristic size of the beam in the x direction and proportional to the beam width w. Thus, the propagation constant $\beta = \eta^\alpha\beta_0$ is proportional to η^α or $w^{-\alpha}$, while the soliton power P_s is proportional to $\eta^{\alpha-1}$ or $w^{1-\alpha}$. Therefore, for a fixed α, solitons with different widths or propagation constants can be scaled to an identical profile.

When $\alpha = 2$, Eq. (1) has a stable sech-form soliton solution [30]:

$$\Psi(x, z) = \eta\,\text{sech}(\eta x)\exp(i\eta^2 z/2). \quad (4)$$

For other α values, we did not find the precise analytical soliton solutions. Therefore, we numerically solve Eq. (2) using the accelerated imaginary-time evolution method [31]. Typical intensity profiles of solitons for beam width $w = 1$ and the corresponding spectra are presented in Figs. 1(a) and 1(b), respectively. Here we define the soliton rms width w as

$$w^2 = 2\left[\frac{\int x^2|\Psi(x, z)|^2 dx}{P} - \left(\frac{\int x|\Psi(x, z)|^2 dx}{P}\right)^2\right]. \quad (5)$$

We note that either the soliton intensity or its spectrum gives a sech-like solution as α tends to 2. When α approaches 1, the soliton has a Lorentz-like profile, whose spectrum is evidently close to the exponential-decay shape, as shown in Fig. 1(b). For a fixed α, the relations of $P_s \propto w^{1-\alpha}$ and $\beta \propto w^{-\alpha}$ are validated by our numerical results, which are fitted by the curves in the form of power-law function.

Now we use the variational method [32] to study the nonlinear dynamics of the FSE. For simplicity, we assume a trial solution in the Gaussian form:

$$\Psi(x, z) = A(z)\exp[ib(z)]\exp\left\{-\frac{x^2}{2w^2(z)}[1 + iC(z)]\right\}, \quad (6)$$

where A is the amplitude, b is the phase of amplitude, w is the beam width, and C stands for the normalized phase-front curvature, the so-called spatial chirp of the beam. Using the Lagrangian density function for the FSE given in Ref. [33], and following the standard procedures of the variational method [32], we find the evolutionary equations for the parameters A, b, C, and w:

$$\frac{dA}{dz} = \frac{A\alpha C}{2\sqrt{\pi}w^\alpha}\Gamma_\alpha(1 + C^2)^{(\alpha/2)-1}, \quad (7)$$

$$\frac{db}{dz} = \frac{5\sqrt{2}}{8}A^2 + \frac{(\alpha - 2)(C^2 - 1) - 4}{4\sqrt{\pi}w^\alpha}\Gamma_\alpha(1 + C^2)^{(\alpha/2)-1}, \quad (8)$$

$$\frac{dC}{dz} = \frac{A^2}{\sqrt{2}} - \frac{\alpha}{\sqrt{\pi}w^\alpha}\Gamma_\alpha(1 + C^2)^{\alpha/2}, \quad (9)$$

$$\frac{d(A^2 w)}{dz} = 0, \quad (10)$$

where $\Gamma_\alpha = \Gamma(\frac{\alpha+1}{2})$ and $\Gamma(\cdot)$ is the gamma function. Equation (10) implies the invariant quantity of the beam power $P \equiv \sqrt{\pi}A^2 w$ during propagation. For a stationary soliton solution, we have

$$A^2 = \sqrt{\frac{2}{\pi}}\alpha\Gamma_\alpha w^{-\alpha}, \quad (11)$$

$$P_s = \sqrt{2}\alpha\Gamma_\alpha w^{1-\alpha}, \quad (12)$$

$$\beta = \frac{2\alpha - 1}{02\sqrt{\pi}}\Gamma_\alpha w^{-\alpha}, \quad (13)$$

and $C = 0$, where $\beta = b/z$ is the propagation constant. Note that here the relations of $P_s \propto w^{1-\alpha}$ and $\beta \propto w^{-\alpha}$ are obtained again.

We plot the curves of soliton power P_s and propagation constant β as functions of the Lévy index α in Figs. 1(c) and 1(d) for different beam widths, comparing with the numerical results. The discrepancy between the analytical (curves) and numerical results (symbols) is relatively small for large α, especially for the soliton power P_s, while that becomes larger when α decreases to 1. The main reason for this discrepancy is that the profiles of Gaussian trial solution are more similar to the sech types than the Lorentz ones.

We also investigate the stabilities of solitons by a standard linear-stability analysis. We consider the perturbed stationary
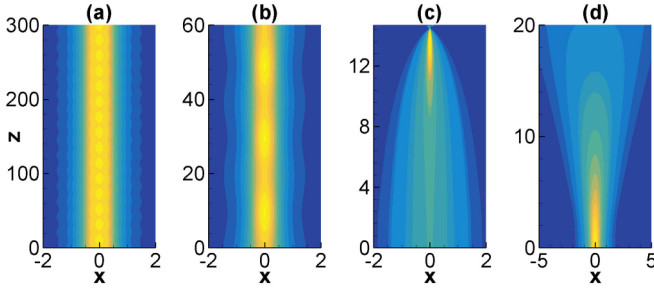
FIG. 2. Simulations of solitons with (a) 1% random-noise perturbations for $\alpha = 1.2$, (b),(c) a 1% increased initial amplitude for $\alpha = 1.2$ and $\alpha = 1.0$, and (d) a 4% decreased initial amplitude for $\alpha = 1.0$.

solution form as

$$\Psi(x, z) = \{\psi(x) + [u(x) + v(x)] \exp(\lambda z)$$
$$+ [u^*(x) - v^*(x)] \exp(\lambda^* z)\} \exp(i\beta z), \quad (14)$$

where $u(x), v(x) \ll 1$, and λ is the eigenvalue of perturbations. Inserting this perturbed solution in Eq. (1), we obtain the linear-stability eigenvalue problem,

$$i\left[-\frac{1}{2}\left(-\frac{\partial^2}{\partial x^2}\right)^{\alpha/2} v - \beta v + \psi^2 v\right] = \lambda u, \quad (15)$$

$$i\left[-\frac{1}{2}\left(-\frac{\partial^2}{\partial x^2}\right)^{\alpha/2} u - \beta u + 3\psi^2 u\right] = \lambda v, \quad (16)$$

which can be numerically solved by the Fourier collocation method [34]. Except for the case of $\alpha = 1$, all solitons contain purely imaginary eigenvalues and thus are stable.

This prediction is confirmed by performing numerical simulations of Eq. (1) based on the split-step Fourier method. The numerical solutions added with 1% random-noise perturbations are used as incident profiles. The example of stable propagation is presented in Fig. 2(a). We also performed numerical simulations with a 1% increased initial amplitude. When $1 < \alpha \leqslant 2$, we find that the beam undergoes a stable oscillation and behaves like a breather [see Fig. 2(b)]. The on-axis intensity initially increases and then undergoes sine-like oscillations, as shown in Fig. 3(a).
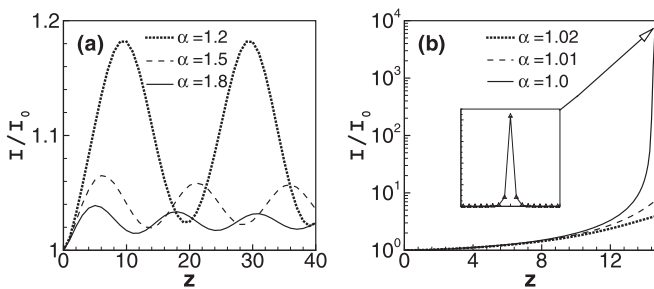
FIG. 3. Normalized on-axis intensities versus the propagation distance for different α values when the solitons with a 1% increased initial amplitude. Here $I_0 = I(0)$. The inset in (b) shows the intensity profile of a beam nearby the singularity.

III. SELF-FOCUSING AND WAVE COLLAPSE

However, for $\alpha = 1$, the beam propagates in an unstable fashion and particularly exhibits the wave collapse property. Figure 2(c) shows that the beam self-focuses to a very small size. Its on-axis intensity has no chance to oscillate and directly grows exponentially to a very high value (about 10^4 times initial intensity), as shown in Fig. 3(b). The inset of Fig. 3(b) shows the final profile of the beam. We can see that within the beam there are only three points, which are ineffective for sampling the optical beam. If the simulation uses much denser sampling points, the final on-axis intensity can grow to a higher value. Therefore, we can expect that the on-axis intensity can rise to an unlimited value (singularity). This phenomenon is identical to the wave collapse occurring in the nonlinear system which is governed by the (1+2)-D traditional NLSE [1–4]. Here we demonstrate that the wave collapse can take place in the (1+1)-D FSE when $\alpha = 1$. However, from a physical point of view, such collapse cannot proceed indefinitely. Recall that in the NLSE, extreme physical processes, which can suppress or even completely eliminate collapse, must be taken into account when close to the singularity [2,3]. The most important one is the nonparaxiality, which should be also included in the FSE as the envelope suddenly increases along the propagation distance. Therefore, Eq. (1) is drastically simplified but still a good approximate model before the singular dynamics appear.

Using the variational method with the trial solution given by Eq. (6), we obtain the evolutions of the on-axis intensity $I(z) \equiv A^2(z)$ and the chirp parameter $C(z)$ for $\alpha = 1$, which are governed by

$$\frac{dy}{dZ} = \frac{y^2}{y_0} \frac{C}{\sqrt{1 + C^2}}, \quad (17)$$

$$\frac{dC}{dZ} = y - \frac{y}{y_0}\sqrt{1 + C^2}. \quad (18)$$

Here $Z = z/Z_r$, where $Z_r = \sqrt{\pi} w_0$ is the effective diffraction length and $w_0 = w(0)$; $y = I(z)/I_c$ is the normalized on-axis intensity and $y_0 = y(0) = P/P_c$, where $I_c = P_c/\sqrt{\pi} w_0$ is the on-axis intensity for a soliton given by Eq. (11). Note that here $P_c = \sqrt{2}$ is not only the soliton power for $\alpha = 1$ [see Fig. 1(c)], but also the critical power for self-focusing as we will see below. The critical power is independent of the beam width, like its counterpart in the (1+2)-D NLSE. The solutions of Eqs. (17) and (18) can be found as

$$C(Z) = C_0 + \left(y_0 - \sqrt{1 + C_0^2}\right)Z, \quad (19)$$

$$y(Z) = y_0\left(y_0 - \sqrt{1 + C_0^2}\right)\frac{y_0 + \sqrt{1 + C^2}}{y_0^2 - 1 - C^2}, \quad (20)$$

where $C_0 = C(0)$ is the initial spatial chirp. It is obvious that when $y_0 > 1$, (i.e., $P > P_c$), the on-axis intensity y increases to infinity at the collapse distance

$$Z_f = \frac{\sqrt{y_0^2 - 1} - C_0}{y_0 - \sqrt{1 + C_0^2}}. \quad (21)$$

The collapse distance is only dependent on the incident power $y_0 = P/P_c$ and the initial chirp C_0. The wave collapse cannot
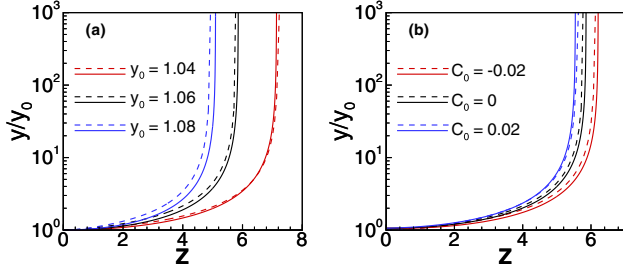
FIG. 4. Normalized on-axis intensity, y/y_0, as a function of normalized distance, Z, with (a) $C_0 = 0$ and (b) $y_0 = 1.06$. Solid curves denote the analytical results obtained by the variational method; dashed curves, the numerical results.

occur if $C_0 < -\sqrt{y_0^2 - 1}$, which means that the incident beam has a strong divergent wave front to conquer the self-focusing effect.

We compare y/y_0 obtained from the variational method [Eq. (20)] with that of the numerical simulation in Fig. 4. For the numerical results, the effective diffraction length $Z_r \approx 0.44\sqrt{\pi}w_0$ is evaluated by numerical fitting for the collapse distance. This discrepancy is mainly caused by the difference of profile between the Gaussian trial solution in the variational method and the Lorentz-like numerical one. Except for the value of Z_r, it is evident that the evolutionary behaviors of numerical and analytical results are the same. As shown in Fig. 4, the collapse distance is shortened with increasing y_0, because the larger power induces a stronger self-focusing effect. For a fixed y_0, the collapse distance is shortened for a convergent wave front ($C_0 > 0$) while lengthened for a divergent one ($C_0 < 0$).

Similar to the case of a (1+2)-D beam in a NLSE, here we can understand the dynamics of a (1+1)-D beam by considering the power conservation and the competition between the linear diffractive action and the nonlinear self-focusing action [35,36]. Let us first consider a (1+1)-D beam for the classical case of $\alpha = 2$. Using the power-conservation law, the nonlinear self-focusing action is then proportional to $1/w$, for it is proportional to $|A|^2$, while the diffraction action is proportional to $1/w^2$. When the beam size decreases due to the self-focusing, both the self-focusing action ($\propto 1/w$) and the diffraction action ($\propto 1/w^2$) become stronger. However, the latter increases faster and then overcomes the former. Therefore the beam will diffract. Conversely, as the beam diverges on

diffraction, the diffraction action becomes weak more rapidly than the self-focusing action and the beam is focused again. Consequently, the beam will diverge and converge periodically around an equilibrium (soliton) state, i.e., the soliton is stable when $\alpha = 2$. In fact, all the cases $1 < \alpha \leqslant 2$ reach the same conclusion as their diffraction actions are both proportional to $1/w^\alpha$, which is also confirmed by the above stability analysis.

However, for the limit case of $\alpha = 1$, the diffraction action is proportional to $1/w$ and becomes the same as the nonlinear self-focusing action. When small deviations initially cause the beam to diverge, with both the diffractive action and the self-focusing action weakening synchronously, the self-focusing action cannot counterbalance the divergence and the beam may diffract to infinity [see Fig. 2(d)]. But when the beam converges at the beginning, the diffraction action cannot stop the convergence and the beam may focus to a singularity. As a result, the (1+1)-D soliton is unstable and tends to collapse at $\alpha = 1$.

IV. CONCLUSION

In conclusion, we investigate the nonlinear dynamics of a (1+1)-D beam in the FSE with the Kerr nonlinearity. We analytically and numerically obtain the relations between the soliton power, the width, and the propagation constant, which are dependent on the Lévy index α. All solitons are stable for $1 < \alpha \leqslant 2$. When $\alpha = 1$, it is found that the beam undergoes a catastrophic collapse, which can be understood by considering the power conservation and the competition between the linear effect and the nonlinear effect. Based on the variational method with a Gaussian-form solution, the analytical expression of the collapse distance is obtained. Numerical results confirm that it characterizes the general tendency of beam behavior.

Our results about the optical soliton, self-focusing, and wave collapse in the FSE can be experimentally verified based on the methods discussed in Ref. [20]. We believe that our study is helpful to understand the FSE, and may have potential applications in nonlinear optical signal processing, and other areas connected with the Kerr effect. In addition, our study may open a way to investigate other fractional processes.

[1] Y. R. Shen, Self-focusing: Experimental, Prog. Quantum Electron. **4**, 1 (1975).

[2] J. H. Marburger, Self-focusing: Theory, Prog. Quantum Electron. **4**, 35 (1975).

[3] L. Bergé, Wave collapse in physics: Principles and applications to light and plasma waves, Phys. Rep. **303**, 259 (1998).

[4] P. L. Kelley, Self-Focusing of Optical Beams, Phys. Rev. Lett. **15**, 1005 (1965).

[5] G. A. Askar'yan, Effects of the gradient of a strong electromagnetic beam on electrons and atoms, Zh. Eksp. Teor. Fiz. **42**, 1567 (1962) [Sov. Phys. JETP **15**, 1088 (1962)].

[6] R. Y. Chiao, E. Garmire, and C. H. Townes, Self-Trapping of Optical Beams, Phys. Rev. Lett. **13**, 479 (1964).

[7] P. Lallemand and N. Bloembergen, Self-Focusing of Laser Beams and Stimulated Raman Gain in Liquids, Phys. Rev. Lett. **15**, 1010 (1965).

[8] E. Garmire, R. Y. Chiao, and C. H. Townes, Dynamics and Characterisics of the Self-Trapping of Intense Light Beams, Phys. Rev. Lett. **16**, 347 (1966).

[9] S. N. Vlasov, V. A. Petrishchev, and V. I. Talanov, Averaged description of wave beams in linear and nonlinear media (the method of moments), Izv. Vys. Uchebn. Zaved. Radiofiz. **14**, 1353 (1971) [Radiophys. Quantum Electron. **14**, 1062 (1971)].

[10] A. Y. Wong and P. Y. Cheung, Three-Dimensional Self-Collapse of Langmuir Waves, Phys. Rev. Lett. **52**, 1222 (1984).

[11] C. A. Sackett, J. M. Gerton, M. Welling, and R. G. Hulet, Measurements of Collective Collapse in a Bose-Einstein Condensate with Attractive Interactions, Phys. Rev. Lett. **82**, 876 (1999).

[12] P. P. Banerjee, A. Korpel, and K. E. Lonngren, Self-refraction of nonlinear capillary-gravity waves, Phys. Fluids **26**, 2393 (1983).

[13] M. Houbier and H. T. C. Stoof, Stability of Bose condensed atomic ^{7}Li, Phys. Rev. A **54**, 5055 (1996).

[14] C. Klein, C. Sparber, and P. Markowich, Numerical study of fractional nonlinear Schrödinger equations, Proc. R. Soc. London, Ser. A **470**, 20140364 (2014).

[15] N. Laskin, Fractional quantum mechanics and Lévy path integrals, Phys. Lett. A **268**, 298 (2000).

[16] N. Laskin, Fractional quantum mechanics, Phys. Rev. E **62**, 3135 (2000).

[17] N. Laskin, Fractional Schrödinger equation, Phys. Rev. E **66**, 056108 (2002).

[18] B. Guo and D. Huang, Existence and stability of standing waves for nonlinear fractional Schrödinger equations, J. Math. Phys. **53**, 083702 (2012).

[19] J. Dong and M. Xu, Some solutions to the space fractional Schrödinger equation using momentum representation method, J. Math. Phys. **48**, 072105 (2007).

[20] S. Longhi, Fractional Schrödinger equation in optics, Opt. Lett. **40**, 1117 (2015).

[21] Y. Zhang, H. Zhong, M. R. Belić, N. Ahmed, Y. Zhang, and M. Xiao, Diffraction-free beams in fractional Schrödinger equation, Sci. Rep. **6**, 23645 (2016).

[22] Y. Zhang, X. Liu, M. R. Belić, W. Zhong, Y. Zhang, and M. Xiao, Propagation Dynamics of a Light Beam in a Fractional Schrödinger Equation, Phys. Rev. Lett. **115**, 180403 (2015).

[23] L. Zhang, C. Li, H. Zhong, C. Xu, D. Lei, Y. Li, and D. Fan, Propagation dynamics of super-Gaussian beams in fractional Schrödinger equation: From linear to nonlinear regimes, Opt. Express **24**, 14406 (2016).

[24] Y. Zhang, H. Zhong, M. R. Belić, Y. Zhu, W. Zhong, Y. Zhang, D. N. Christodoulides, and M. Xiao, PT symmetry in a fractional Schrödinger equation, Laser Photon. Rev. **10**, 526 (2016).

[25] W.-P. Zhong, M. R. Belić, B. A. Malomed, Y. Zhang, and T. Huang, Spatiotemporal accessible solitons in fractional dimensions, Phys. Rev. E **94**, 012216 (2016).

[26] C. Huang and L. Dong, Gap solitons in the nonlinear fractional Schrödinger equation with an optical lattice, Opt. Lett. **41**, 5636 (2016).

[27] Y. Hong and Y. Sire, A new class of traveling solitons for cubic fractional nonlinear Schrödinger equations, Nonlinearity **30**, 1262 (2017).

[28] J. Xiao, Z. Tian, C. Huang, and L. Dong, Surface gap solitons in a nonlinear fractional Schrödinger equation, Opt. Express **26**, 2650 (2018).

[29] D. Zhang, Y. Zhang, Z. Zhang, N. Ahmed, Y. Zhang, F. Li, M. R. Belić, and M. Xiao, Unveiling the link between fractional schrödinger equation and light propagation in honeycomb lattice, Ann. Phys. (Berlin) **529**, 1700149 (2017).

[30] G. P. Agrawal, *Nonlinear Fiber Optics* (Elsevier, New York, 2007).

[31] J. Yang and T. I. Lakoba, Accelerated imaginary-time evolution methods for the computation of solitary waves, Stud. Appl. Math. **120**, 265 (2008).

[32] B. A. Malomed, Variational methods in nonlinear fiber optics and related fields, Prog. Opt. **43**, 71 (2002).

[33] S. I. Muslih, O. P. Agrawal, and D. Baleanu, A fractional Schrödinger equation and its solution, Int. J. Theor. Phys. **49**, 1746 (2010).

[34] J. Yang, *Nonlinear Waves in Integrable and Nonintegrable Systems* (SIAM, Philadelphia, 2010).

[35] A. Hasegawa and Y. Kodama, *Solitons in Optical Communications* (Clarendon, Oxford, 1995).

[36] Q. Guo, D. Lu, and D. Deng, Nonlocal spatial optical solitons, in *Advances in Nonlinear Optics*, edited by X. Chen, Q. Guo, W. She, H. Zeng, and G. Zhang (De Gruyter, Boston, Berlin, 2015), pp. 227–305.